Desalination and Water Treatment
www.deswater.com

doi:10.5004/dwt.2021.26589

211 (2021) 267–279
January

Treatment of aqueous selenocyanate ($SeCN^-$) using combined TiO_2 photocatalysis and 2-line ferrihydrite adsorption

Sameh A.A. Ahmed, Muhammad S. Vohra*

Environmental Engineering Program, Civil and Environmental Engineering Department, King Fahd University of Petroleum and Minerals, Dhahran, Saudi Arabia, Tel. +(966) 013-860-2854; emails: vohra@kfupm.edu.sa (M.S. Vohra), same7.araby@gmail.com (S.A.A. Ahmed)

Received 13 September 2019; Accepted 27 September 2020

ABSTRACT

The presence of selenocyanate ($SeCN^-$) species in some specific industrial wastewater streams including those from the crude oil refineries and mining industries, pose a risk to human and animal health. The present work thus investigated the treatment of selenocyanate contaminated water using combined TiO_2 photocatalysis and 2 line ferrihydrite (2LFh) adsorption system. The X-ray diffraction findings indicated the synthesized 2LFh to be in the amorphous state, whereas the Fourier transform infrared results showed several Fe- and O-based groups onto the 2LFh surface. During selenocyanate removal using the above-mentioned combined system, the TiO_2 photocatalysis initiated the selenocyanate complex degradation with selenite and selenate species appearing over 360 min reaction time. This was followed by the adsorption of released selenium species onto 2LFh. Results from the respective TiO_2 photocatalysis and 2LFh adsorption studies showed that the combination of the two systems through efficient, but was affected by the process control variables including pH. A complete selenium removal was noted at pH 5, whereas the selenium removal decreased significantly with an increase in the process pH. This was attributed to lower adsorption of released selenium species onto 2LFh. The response surface methodology (RSM) modeling also showed reasonable estimates for the aqueous phase selenocyanate removal under a varying set of operational conditions.

Keywords: 2LFh; TiO_2; Selenocyanate; Selenite; Selenate

1. Introduction

The selenium species occurs in the natural environment in several oxidation states [1–3]. For example, the oxyanions selenite (SeO_3^{2-}) and selenate (SeO_4^{2-}) are usually noted under oxidizing environmental conditions whereas the Se(0) and Se(–II) species exist under reducing anaerobic conditions. Though the selenium species is an essential micronutrient for human health, however, at elevated intakes it is toxic. For example, the gastrointestinal and nervous systems are negatively affected upon adverse selenium exposures [2]. Hence strict selenium regulatory limits have been promulgated both for the drinking water and wastewater discharge. The US EPA selenium regulations include 50 ppb for the drinking water and 5 ppb as a discharge threshold limit [3,4]. Additionally, industrial wastewater generated from sources such as crude oil refineries and power plants that use fossil fuels may have another selenium species, that is, selenocyanate ($SeCN^-$) that is also toxic to humans [4–8]. Furthermore, the selenocyante species also poses a treatment challenge and the removal of selenocyanate from respective wastewater streams remains a difficult task. So far several remediation methods have been investigated to remove selenite, selenate, and selenocyanate from polluted water bodies including adsorption [9–13], advanced oxidation processes [1,14–18], electrocoagulation [19] ion exchange [20], and specific iron-based

* Corresponding author.

systems [21,22]. For example, Das et al. [11] report a comparative study between 2 line ferrihydrite (2LFh), goethite, and lepidocrocite for aqueous phase selenate adsorption, noted 2LFh to be the most effective and efficient adsorbent. Furthermore, Meng et al. [21] report the successful application of zero-valent iron (ZVI) for selenocyanate reduction to elemental selenium followed by its precipitation. Another study reported that the selenocyanate complex could be destroyed using a specific chemical oxidant followed by adsorption of released selenium species onto iron precipitates [22]. Nevertheless, as the limitations regarding selenocyanate species removal remain both a concern and a challenge, some new, and innovative combinations of existing selenium removal technologies are needed. For example, the destruction of selenocyanate complex using TiO_2 assisted photocatalysis [17,18] can be combined with a specific adsorption system [9–11,13,20,23,24] to remove the respective released selenium species from the aqueous phase. To that end, 2LFh has been reported to interact with several species including arsenic [25–32], arsenic and nickel [33], chromium [34–36], lanthanide [37,38], copper, cadmium, lead and zinc [39,40], fluoride [41], molybdenum and vanadium [42], dye methyl orange [43], airborne pollutants including acetaldehyde, carbon dioxide and ozone [44–46], phosphate [47], thiocyanate [48], and selenium [11,24,49,50]. Considering this, the present work investigated the efficiency of combined TiO_2 based photocatalysis that can destroy the selenocyanate complex followed by an uptake of the resulting selenite and selenate species by the aforementioned 2LFh adsorbent. The application of the respective combined system for the treatment of aqueous selenocyanate was studied under different process conditions and details are reported in the following sections.

2. Materials and methods

2.1. Materials

Reagent grade chemicals were used for all experimental work including KSeCN (ALDRICH, USA), K_2SeO_4 (ALDRICH, USA), Na_2SeO_3 (ALDRICH, USA), $FeCl_3$ (BDH, England), TiO_2 powder (P25, DEGUSSA, Germany), $NaHCO_3$ (BDH, England), Na_2CO_3 (BDH, England), HCl (FISHER, USA), H_2SO_4 (FISHER, USA), HNO_3 (FISHER, USA), and NaOH (FISHER, USA).

2.2. Synthesis of 2-Line Ferrihydrite

To synthesize 2LFh, 500 mL of 0.2 M of $FeCl_3$ was first prepared followed by micro-level titration with NaOH till reaching pH 7–8 [11,36]. The obtained precipitate was then centrifuged and subsequently washed with high purity water followed again by centrifuge; this procedure was repeated multiple times to clean 2LFh precipitate from any chloride impurities. After that, the solids were freeze dried (FreeZone 4.5 L Benchtop, LABCONCO, USA) and then stored (till further analysis) in a refrigerator.

2.3. Experimental procedures

The selenocyanate adsorption isotherm study was completed using initial selenocyanate concentrations between 2.5 and 50 mg/L while the selenite and selenate (single system; pH effect) adsorption studies were completed at 20 mg/L. The experimental batch solutions were prepared using high purity water (CORNING Mega Pure™ System) and stock solutions of respective target pollutants. The pH was adjusted using NaOH or HCl solutions. During the adsorption studies, the respective systems were subjected to magnetic stirring and also covered with an aluminum foil. All systems were allowed to reach equilibrium and each sample was first centrifuged and then filtered using a 0.2 μm filter paper for further analysis.

The photocatalysis cum adsorption experiments were completed using a 1,000 mL Pyrex glass batch type reactor (Fig. 1). For each experiment, a 1,100 mL of test batch solution was first prepared followed by a 100 mL sample taken as a blank to assess the initial selenocyanate concentration. After that 1 g/L TiO_2 was added to the remaining 1,000 mL with constant magnetic stirring. The desired 2LFh amount was then added and pH adjusted using NaOH or HCl solutions. The test solution was subsequently poured into a batch reactor (Fig. 1) that was covered with an aluminum foil and allowed to equilibrate for 30 min and a second blank sample was then taken to quantify any initial selenocyanate adsorption. The test suspension was then exposed to a 15 W low-pressure UV lamp with a wavelength ~352 nm (F15T8-BLB, Sankyo Denki, Japan). The mean temperature of TiO_2 suspension during the photocatalysis experiments was near 26°C, which did not require a cooling system [14]. Samples were taken at specific time intervals during the photocatalysis cum adsorption study and analyzed for the target selenium species as outlined below.

2.4. Analytical methods

The X-ray diffraction (XRD) results for 2LFh were obtained using ADX 2500 XRD setup (Angstrom-Advanced, USA). Diffraction data were acquired at 1°/min step with an angular range of 2θ from 10° to 80°. The solid-state infrared spectra for 2LFh was obtained using the Fourier transform infrared (FTIR) spectrometer (16F PC FTIR, Perkin Elmer, USA) using solid potassium bromide (KBr) pellets and within 650–4,000 cm^{-1} range.

For the aqueous selenium species analyses, all respective samples were first duly filtered using a 0.2 μm filter (WHATMAN, Germany). The total selenium analyses were completed using an atomic absorption spectrometer setup (Perkin Elmer, USA). Furthermore, the aqueous selenite/SeO_3^{2-}, selenate/SeO_4^{2-}, and selenocyanate/$SeCN^-$ species analyses were completed using advanced ion chromatography equipment (Metrohm, Switzerland). The eluent composition was 3.2 mM Na_2CO_3/1 mM $NaHCO_3$ and the column was Metrosep Anion Dual 2 (Metrohm, Switzerland). The respective equipment was duly calibrated before each run.

2.5. Response surface methodology

The Box–Behnken design (BBD) type response surface methodology (RSM) is an established technique to optimize the design and modeling of a given research endeavor with the least number of experiments [51]. This approach

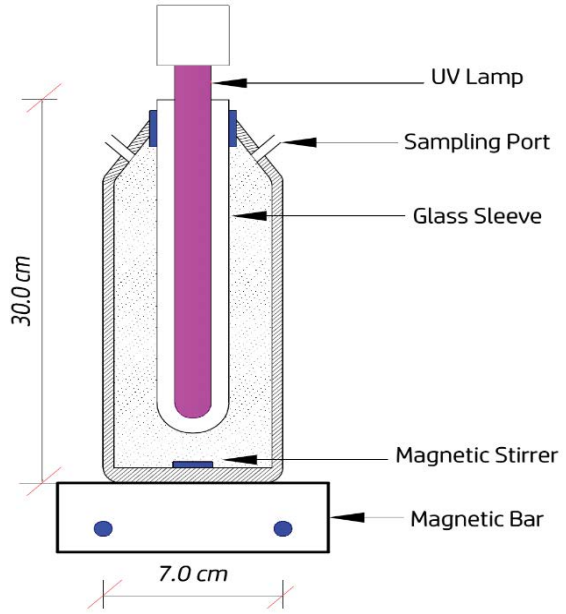

Fig. 1. Reactor used for the combined TiO_2 photocatalysis and 2LFh adsorption experiments.

has also been successfully used for environmental engineering applications [52,53]. In the present work, the three independent factors, that is, pH, 2LFh dose, and initial selenocyanate concentration, were examined during RSM modeling design. Each factor was equally spaced, that is, pH at 5, 7, and 9, 2LFh amount at 0.5, 1, and 1.5 g/L, and the initial selenocyanate concentration at 10, 15, and 20 mg/L. The Design-Expert software was used to analyze the response, that is, the total selenium removal after 360 min, as a function of above-mentioned factors.

3. Results and discussion

3.1. Characterization of 2-Line Ferrihydrite

The synthesized 2LFh product was first characterized using the XRD technique. The respective results (Fig. 2) revealed two broad peaks at 35° and 63°, indicating an amorphous iron oxide, as also reported earlier by Rani and Tiwari [54] and Snow et al. [55]. Brayner et al. [56] also noted a similar XRD pattern for a biosynthesized 2LFh. Furthermore, the attenuated total reflection-Fourier transform infrared (ATR-FTIR) spectra of synthesized 2LFh from 650 to 4,000 cm^{-1} (Fig. 2) shows a broad peak at 3,230 cm^{-1} corresponding to the O–H presence. Jeong et al. [57]

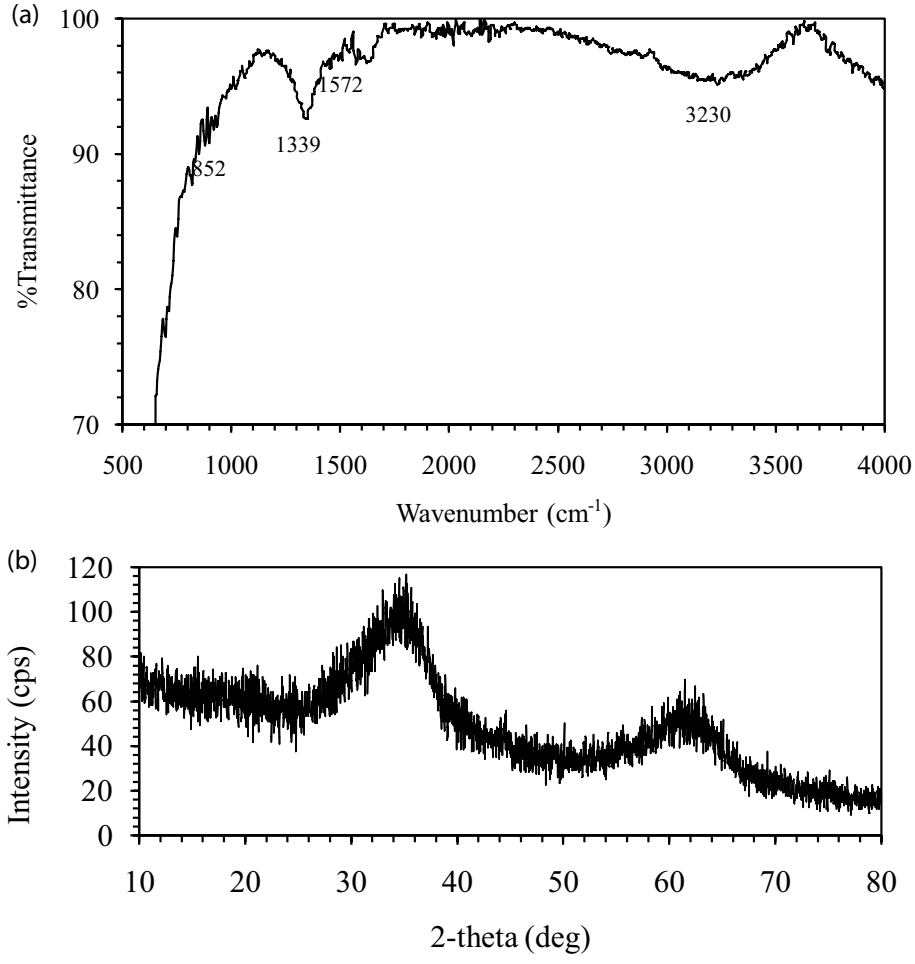

Fig. 2. (a) ATR-FTIR spectrum of 2LFh sample and (b) XRD results for synthetized 2LFh sample.

ascribed the respective peak to structural OH at the 2LFh surface. Furthermore, the peaks at 1,339 and 1,572 cm^{-1} are assigned to Fe–OH and Fe–O groups, respectively [40]. Such specific groups at the 2LFh surface are expected to initiate an adsorption based uptake of target pollutants, that is, the selenium based species. These details will be invoked later to explain the selenium removal trends from the present work.

3.2. Adsorption isotherm results

The uptake of aqueous selenocyanate by 2LFh was initially studied to realize selenocyanate equilibrium between the bulk aqueous phase and the 2LFh adsorbent surface. The adsorption isotherm as given in Fig. 3 relates the respective adsorption capacity (q_e) to equilibrium selenocyanate concentration (C_e). The respective results show that selenocyanate adsorption onto 2LFh surface follows a typical Langmuir type trend, that is, a gradual increase in the adsorption capacity q_e is noted with an increment in the C_e value. The adsorption capacity also increases from 0.89 to 3 mg/g till reaching a plateau, which supports a monolayer coverage. Initially, an increase in the selenocyanate adsorption with an increase in its initial aqueous concentration, could result because of a higher selenocyanate mass transfer driving force from bulk aqueous to bulk solid phase. Nevertheless, as the available sites reach a saturation state, the net adsorption also stabilizes because of equilibrium between the 2LFh surface and aqueous phase selenocyanate species [39,47]. These trends were first modeled using the Langmuir isotherm is given by Eq. (1) and its linearized form as per Eq. (2) [53]:

$$q_e = \frac{q_m K_L C_e}{1 + K_L C_e} \tag{1}$$

$$\frac{C_e}{q_e} = \frac{1}{K_L (q_m)} + C_e \left(\frac{1}{q_m}\right) \tag{2}$$

where C_e is the equilibrium selenocyanate concentration (mg/L); q_e is the adsorption capacity (mg/g); q_m is the maximum adsorption capacity (mg/g); K_L is the Langmuir constant (L/mg).

Fig. 4 shows that the selenocyanate adsorption data fits well to the Langmuir isotherm with correlation coefficient equal to 0.9993 and a maximum adsorption capacity q_m of 3 mg/g and K_L value equal to 1.51 L/mg. Das et al. [11] noted a qualitatively similar trend for the selenate species adsorption onto 2LFh surface. On the other hand, use of the Freundlich isotherm that assumes a multilayer adsorption onto surface sites did not yield a better fit and hence was not considered. Other 2LFh adsorption studies have also reported a better fit obtained using the Langmuir isotherm [27,29,39,41,48]. Furthermore, some modified 2LFh have also shown a similar trend. For example, Jia et al. [58] who studied fluoride adsorption on to 2LFh-bayerite material report that the Langmuir isotherm fitted well to respective adsorption data. Similar was noted by Zhao et al. [43] for anionic methyl orange dye adsorption onto alginate-2LFh beads. However, Huang et al. [59] who studied cadmium adsorption onto 2LFh report a better modeling fit obtained using the Freundlich isotherm. The authors also report cadmium precipitation at higher pH values. It should be noted that the Freundlich isotherm that considers multilayer surface coverage (as compared to the Langmuir isotherm that considers a monolayer coverage) may well-describe scenarios where an initial complexation of the target contaminant with the 2LFh surface adsorption sites is followed by re-adsorption of dissolved Fe-species onto the existing surface complex that again provides the sites for the target-contaminant complexation. In any case, adsorption of selenocyanate onto 2LFh is better defined using the Langmuir isotherm indicating a monolayer coverage.

3.3. Combined photocatalysis and 2LFh adsorption results

The reactor setup as shown in Fig. 1 was used for all selenocyanate degradation experiments. The initial experiments that were completed using either only UV light or UV light with 2LFh, indicated an insignificant selenocyanate removal. Therefore, a combined process that employs TiO_2 photocatalysis to break down the selenocyanate complex followed by the removal of released selenite and

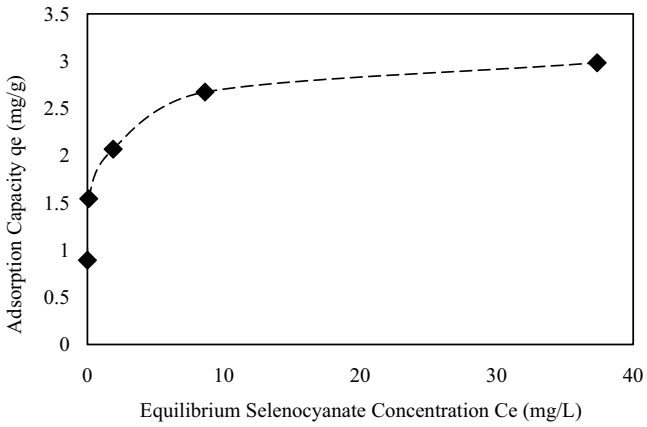

Fig. 3. Adsorption isotherm for selenocyanate uptake by 2LFh (3 g/L 2LFh, pH 5, and 96 h contact time).

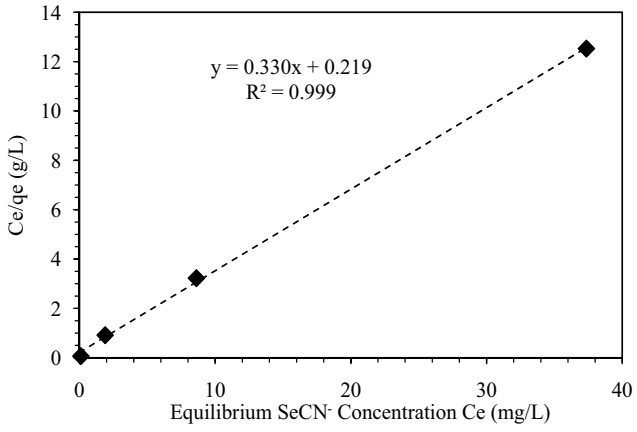

Fig. 4. Langmuir adsorption isotherm for selenocyanate adsorption using 2LFh (3 g/L 2LFh, pH 5, and 96 h contact time).

selenate species via adsorption onto 2LFh, was investigated. Figs. 5a–d show results for the experiments that were completed at pH 5. It is noted that though the TiO_2 only system causes significant selenocyanate removal (Fig. 5b), however, it fails to remove the resulting selenite and selenate species from the aqueous phase whereas use of TiO_2 with 2LFh shows enhanced removal of respective selenium species because of adsorption (Figs. 5c–d). During photocatalysis the destruction of selenocyanate complex is successfully initiated by the hydroxyl radicals ($OH^{\bullet}$) that are produced during photocatalytic degradation (PCD) process [17,18]. Hoffmann et al. [60] elucidated use of TiO_2 during photocatalysis and the respective reaction mechanism are represented by Eqs. (3) and (4):

$$TiO_2 + h\nu \rightarrow e^- + h^+ \quad (3)$$

$$\underline{\mathbf{Ti}}\text{–}OH^- + h^+ \rightarrow \underline{\mathbf{Ti}}\text{–}OH^{\bullet} \quad (4)$$

Eq. (3) shows that upon exposure to an appropriate UV light source, the valence band electrons/e^- in a TiO_2 particle are excited and consequently transferred to the conduction band, resulting in an electron/hole pair (e^-/h^+) formation. Moreover, the h^+ species in the valence band, scavenges an electron from the hydroxyl species (OH^-) adsorbed onto surface of TiO_2 generating hydroxyl radical ($OH^{\bullet}$) (Eq. (4)) that in turn breaks down the selenocyanate complex, eventually converting it first to oxidized selenite and then to selenate species (Fig. 5). Furthermore, in contrast to the previous TiO_2 based systems that report use of reducing agents such as formate to initiate reduction of selenite/selenate to elemental selenium with subsequent selenium precipitation [1,14,16], in the present work the produced oxidized selenium species are removed by adsorption onto 2LFh. In that regard, Fig. 5b shows approximately 85% selenocyanate removal in the initial 2 h and near complete removal at 6 h. However, the total selenium results (Fig. 5a) show that in the absence of 2LFh, only approximately 20% of total selenium is removed, whereas using 2LFh during photocatalysis renders a gradual decrease in total selenium. Also, Fig. 5c that compares the selenite trends shows that in the absence of 2LFh, selenite builds up at an earlier stage to reach 25% at 60 min, followed by a decrease. It should be noted that the respective decrease in selenite is caused because of its conversion to selenate species (and not from adsorption onto TiO_2). However, in the presence of 2LFh, the selenite species builds only up to 4% at 60 min and it then disappears completely (Fig. 5c). Furthermore, Fig. 5d that compares the selenate trends shows a clear difference

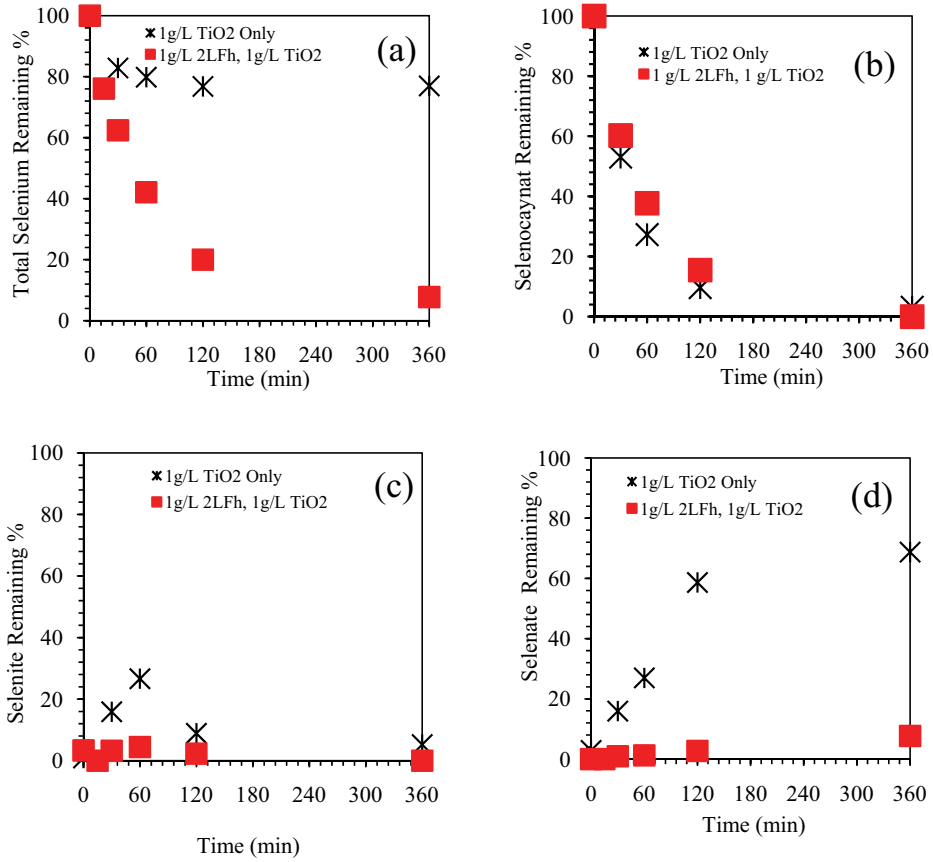

Fig. 5. Comparison between use of TiO_2 only and TiO_2/2LFh during selenocyanate photocatalysis-adsorption based treatment: (a) total selenium trends, (b) selenocyanate trends, (c) selenite trends, and (d) selenate trends (20 mg/L selenocyanate, 1 g/L TiO_2, 1 g/L 2LFh, 15 W UV lamp, and pH 5).

between the without and with 2LFh systems. For the former case, selenate species continues to build reaching up to 65%. On the other hand, in the presence of 2LFh, we note only 7% selenate species remaining at 360 min. These trends clearly show the TiO_2-2LFh process' efficiency for the selenium species removal.

To further clarify the role of pH and considering the pH to be an important process parameter, the effect of pH during TiO_2-2LFh based selenocyanate removal was further investigated at pH 9. The respective results are shown in Figs. 6a–d. For the only TiO_2 experiment, the selenocyanate species disappears quickly within 120 min reaction time (Fig. 6b) along with a significant selenite species build-up (Fig. 6c) and a gradual increase in selenate (Fig. 6d), that is, about 65% and 28% selenite and selenate species, respectively. After 120 min the selenite species starts to decrease gradually while getting oxidized to selenate. However, the results indicate negligible total selenium removal over 360 min reaction time (TiO_2 only results, Fig. 6a). On the other hand, results from the combined TiO_2/2LFh system show more than 90% selenocyanate removal (Fig. 6b) with 10% selenite (Fig. 6c) and 40% selenate (Fig. 6d) still remaining in the aqueous phase. Hence, the addition of 2LFh certainly improves the selenium removal efficiency at pH 9. However, the overall selenium removal at pH 9 is lower because of reduced selenite and selenate adsorption on to 2LFh. In this regard, additional adsorption experiments were conducted to realize the selenite and selenate adsorption behavior onto 2LFh; the respective results are given in Fig. 7. It should be noted that these experiments were conducted for only selenite and only selenate systems. For the single 20 mg/L selenite and 20 mg/L selenate systems at pH values of 5, 7, and 9, the following trend is noted: for the selenite system, approximately 96% selenite removal is noted at pH 5, whereas approximately 56% removal transpires at pH 7 that further reduces to 22% at pH 9. Furthermore, the selenate removal also lowers with an increase in pH, that is, approximately 95% at pH 5, 45% at pH 7, and negligible at pH 9 as shown in Fig. 7. Several studies report the pH_{zpc} of 2LFh to be ~8 [29,40,41,43,48,61]. Hence, the above-mentioned selenite and selenite adsorption trends could be attributed to an increased electrostatic repulsion due to 2LFh tuning anionic at pH above pH_{zpc}. The aforementioned surface functional groups and specifically the OH-based groups (Fig. 2a, section 3.1 – Characterization of 2-Line Ferrihydrite) may contribute to such pH based adsorption trends. Hence, though the 2LFh surface has a special affinity for selenite and selenate species, however, such an affinity also decreases with an increase in the suspension pH. These trends can be explained based on the changes in the 2LFh surface speciation as represented by Eqs. (5) and (6):

$$\underline{\mathbf{Fe}}\text{–}OH_2^+ \leftrightarrow \underline{\mathbf{Fe}}\text{–}OH + H^+ \quad (5)$$

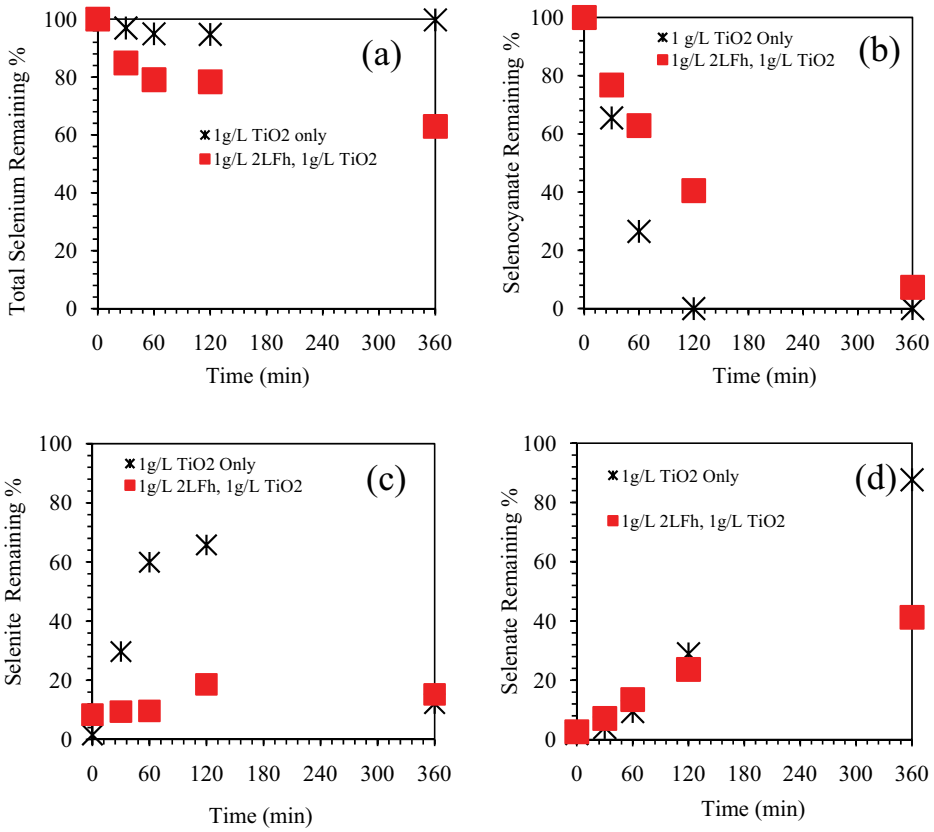

Fig. 6. Comparison between use of TiO_2 only and TiO_2/2LFh during selenocyanate photocatalysis-adsorption based treatment: (a) total selenium trends, (b) selenocyanate trends, (c) selenite trends, and (d) selenate trends (20 mg/L selenocyanate, 1 g/L TiO_2, 1 g/L 2LFh, 15 W UV lamp, and pH 9).

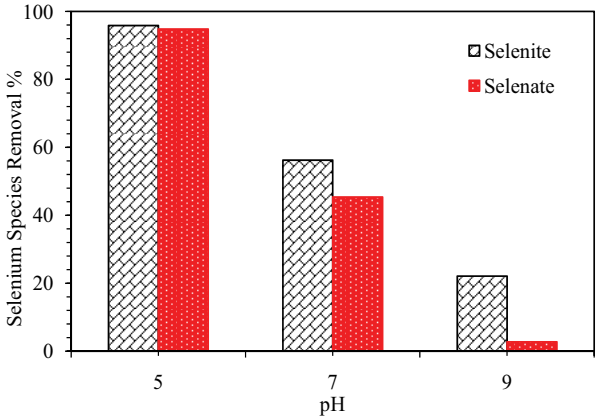

Fig. 7. Adsorption results from single systems: the effect of pH onto adsorption of only 20 mg/L selenite and only 20 mg/L selenate onto 2LFh surface (1 g/L 2LFh and 24 h equilibrium time).

$$\underline{\mathbf{Fe}}\text{–OH} \leftrightarrow \underline{\mathbf{Fe}}\text{–O}^{-} + \text{H}^{+} \quad (6)$$

The above noted reduced selenium removal at high pH values can be explained based on both higher OH^- ion concentration and consequently its competitive adsorption on to 2LFh sites and also an increased anionic nature of 2LFh at the basic pH values (Eq. (6)). On the other hand, the increased selenium removal at low pH values is attributed to respective cationic nature of 2LFh sites (Eq. (5)). However, as the 2LFh surface becomes more negatively charged with an increase in pH, it does not favor the adsorption of anionic selenium species. These findings are similar to those reported in previous studies for 2LFh. Snyder and Um [24] investigated selenite and selenite adsorption onto 2LFh and noted higher selenium removal at pH below 7. Also, Mamun et al. [62] observed a similar trend for Cr(VI) removal using 2LFh. The authors noted higher chromium adsorption at pH 5 compared to pH 7 and attributed it to the positively charged 2LFh surface at acidic pH. Furthermore, the 2LFh based adsorption of anionic arsenate [29], fluoride [41], and thiocyanate species [48] also showed a qualitatively similar pH trend. Several studies report the pH_{zpc} of 2LFh to be ~8 [29,40,41,43,48,61], below which the surface of 2LFh will have a dominant positive charge (Eq. (5)) and in turn will be more conducive for the adsorption of anionic contaminant species. Hence the pH_{zpc} of 2LFh plays an important role during the surface complexation process. On the other hand, Huang et al. [59] who studied cationic cadmium uptake by 2LFh particles noted an increased cadmium uptake with an increase in pH up to 9. The authors attributed the noted reduced cadmium removal at low pH values to higher H^+ ions presence and consequently its competitive adsorption on to 2LFh sites. However, as the 2LFh surface becomes more anionic with an increase in pH, it favors the adsorption of cationic cadmium species. A qualitatively similar adsorption trend was also noted for several other heavy metals including copper, lead, and zinc onto 2LFh, which was explained based on both higher H^+ ion concentration and increased cationic nature of 2LFh at acidic pH values [40]. Juillot et al. [61] also noted a similar pH depended on trend for cationic zinc species uptake by 2LFh with insignificant zinc removal below pH 4–5 whereas at pH 8, a notable zinc removal transpired. Thus, the selenium removal using the combined TiO_2 photocatalysis and 2LFh adsorption process can be duly optimized by controlling the process pH as evident from the results in Figs. 5–7.

Considering the important role of 2LFh in the above-mentioned process, the effect of 2LFh amount onto respective selenium species removal was also investigated. Figs. 8a–d summarizes the comparison between two selenocyanate removal systems completed using 0.5 and 1.5 g/L 2LFh at pH 7. The respective results show only up to 30% total selenium removal using 0.5 g/L 2LFh (Fig. 8a). However, using 1.5 g/L 2LFh, approximately 90% total selenium removal is noted at 360 min. The respective selenite results show small amounts remaining for both 2LFh systems (Fig. 8c) that is qualitatively similar to results from the previous 2LFh systems (Figs. 5 and 6). Fig. 7 also shows a significant selenite adsorption onto 2LFh at pH 7 that supports the selenite removal trends of Fig. 8c. Furthermore, Fig. 8d that compares the selenate results shows the 1.5 g/L 2FLh system to be more effective for selenate removal compared to the 0.5 g/L 2FLh system. The respective 1.5 g/L 2FLh selenate removal findings are also comparable to aforementioned 1 g/L 2LFh selenate removal at pH 5 (Fig. 5d). It should be noted that at 0.5 g/L, the limited 2LFh surface complexation sites will be saturated due to adsorption of selenite and selenate species, causing higher aqueous phase selenate build up (Fig. 8d). On the other hand, at higher 2LFh amount of 1.5 g/L, both selenite and selenate species are simultaneously adsorbed onto 2LFh at higher rate with near complete removal.

The present work was further expanded to investigate the effect of initial selenocyanate concentration onto TiO_2-2LFh process' treatment efficiency. To that end, two additional experiments were completed at 10 mg/L initial selenocyanate and pH 5 and 9, and those findings (along with the 20 mg/L selenocyanate results) are given in Figs. 9 and 10, respectively. Results at pH 5 show that the total selenium removal somewhat decreases with an increase in selenocyanate amount (Fig. 9a); approximately 90% and 80% removal are observed at 120 min reaction time for 10 and 20 mg/L selenocyanate systems, respectively (Fig. 9a). A similar trend is noted for selenocyanate species (Fig. 9b). Nevertheless, the selenite and selenate removal results show no significant effect of initial selenocyanate concentration (Figs. 9c and d, respectively), which could be attributed to their simultaneous adsorption onto 2LFh. Qualitatively similar trends are noted at pH 9 for the total selenium and selenocyanate findings (Figs. 10a and b, respectively). However, the removal of selenite and selenate species is lower (Figs. 10c and d, respectively) that is elucidated based on their reduced adsorption onto 2LFh at higher pH. In summary, the above results show that the use of TiO_2/2LFh based photocatalysis cum adsorption system causing destruction of selenocyanate complex followed by the adsorption of reaction intermediates selenite and selenate onto 2LFh can be successfully employed to treat respective wastewater streams as described in the aforementioned findings. Hence, the application of 2LFh adsorbent along with TiO_2 photocatalysis offers a viable process for the treatment of selenocyanate contaminated waters.

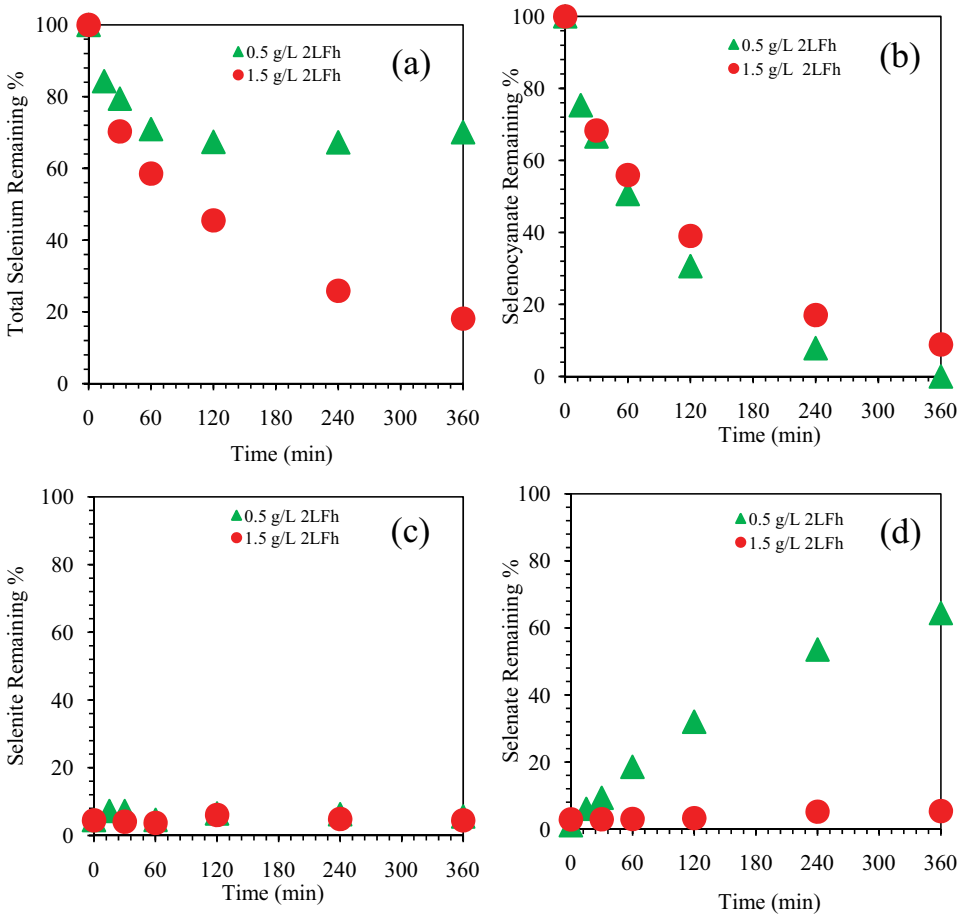

Fig. 8. (a–d) Effect of 2LFh amount onto the removal of (a) total selenium remaining, (b) selenocyanate remaining, (c) selenite remaining, and (d) selenate remaining associated species during destruction of selenocyanate complex using photocatalysis (20 mg/L selenocyanate, 1 g/L TiO_2, 15 W UV lamp, and pH 7).

3.4. RSM modeling

The RSM based modeling for optimization purpose has been used for several environmental engineering applications [16,53]. The RSM approach compares a specific response under varying process conditions (or factors) to optimize the respective process [51]. In this work, the BBD design approach (section 2.5 (Response surface methodology)) was used, which is a special type of RSM technique that considers three factors with three equally spaced levels for the experimental design and response analysis (Table 1). The BBD requires less number of experiments though it is considered as comparable to other methods, for example, the central composite design, which comparatively requires more experiments. In the present work, the effect of three independent factors, that is, 2LFh amount, initial selenocyanate concentration, and pH onto total selenium removal (% at 360 min) was investigated. Results from 13 randomized experimental runs along with the Design-Expert software were used for respective analysis (Table 1). The software employed the least square regression method while fitting the experimental data to the selected polynomial function. Eq. (7) shows the model equation for total selenium removal in terms of coded factors *A*, *B*, and *C*, for 2LFh amount (–1 = 0.5 g/L, 0 = 1 g/L, and +1 = 1.5 g/L), selenocyanate concentration (–1 = 10 mg/L, 0 = 15 mg/L, and +1 = 20 mg/L), and pH (–1 = pH 5, 0 = pH 7, and +1 = pH 9), respectively. Moreover, Table 2 provides analysis of variance (ANOVA) findings and shows the significance level of model and its terms based on the *p*-value. When *p*-value is less than 0.05, it indicates that the model terms are significant in predicting the experimental response.

$$\text{Total selenium removal \%} = +66.61 + 15.73 \times A - 4.46 \times B - 21.79 \times C \quad (7)$$

Typically, the model presented a *p*-value of 0.0094 which is less than 0.05. Thus, it implies that model is significant. Additionally, the model terms *A* and *C* are also statistically significant. Moreover, Eq. (7) shows that the total selenium removal is enhanced at higher 2LFh values, because of higher surface complexation sites for selenium species adsorption. In contrast, the total selenium removal decreases as the initial pH increases. At basic pH values the 2LFh will have a dominant negative surface that causes the 2LFh and anionic selenium to repel each other (Eq. (6)). Nevertheless, at acidic pH the 2LFh is predominantly positive (Eq. (5)), that will

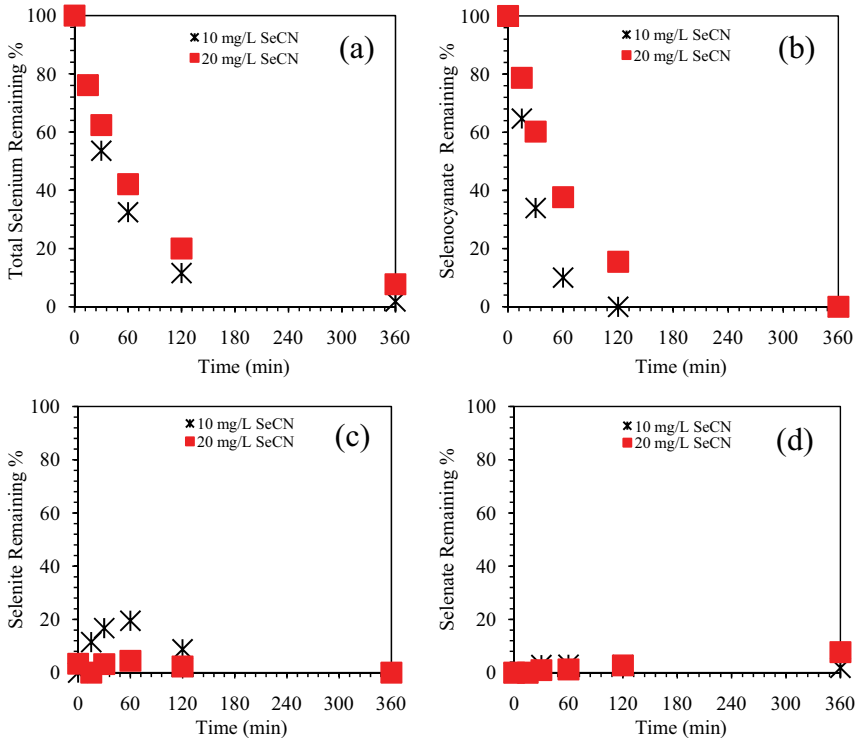

Fig. 9. Selenocyanate removal as a function of its initial concentration (a) total selenium remaining, (b) selenocyanate remaining, (c) selenite remaining, and (d) selenate remaining during the destruction of selenocyanate complex using photocatalysis (1 g/L 2LFh, 1 g/L TiO_2, 15 W UV lamp, and pH 5).

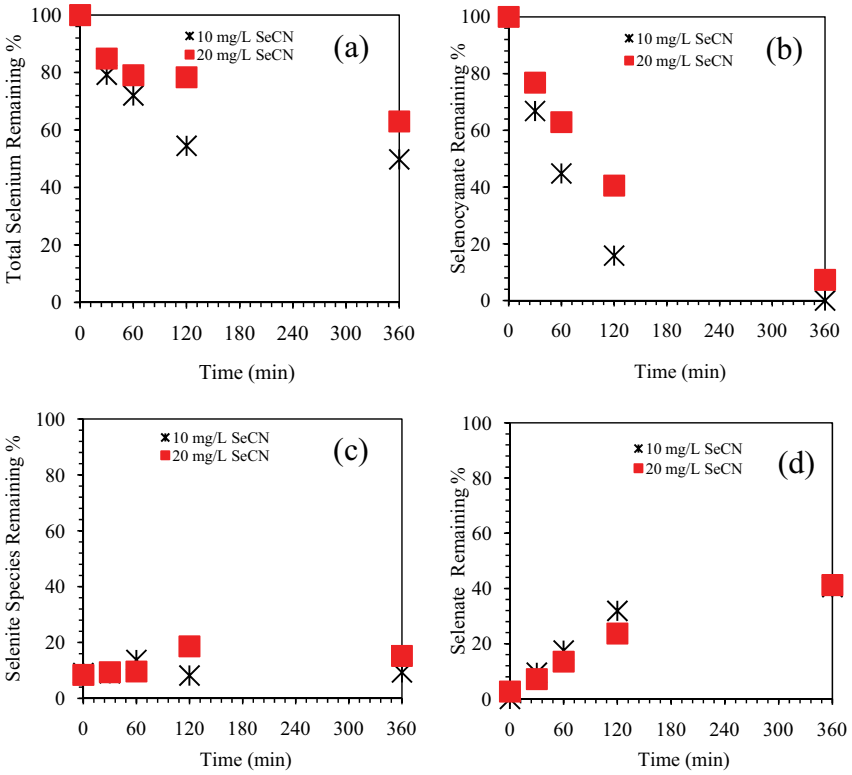

Fig. 10. Selenocyanate removal as a function of its initial concentration (a) total selenium remaining, (b) selenocyanate remaining, (c) selenite remaining, and (d) selenate remaining during the destruction of selenocyanate complex using photocatalysis (1 g/L 2LFh, 1 g/L TiO_2, 15 W UV lamp, and pH 9).

Table 1
RSM-BBD experimental design parameters and total selenium removal

Experiment no.	Factor *A*: 2LFh (g/L)	Factor *B*: selenocyanate (mg/L)	Factor *C*: pH	Response: total selenium removal (% at 360 min)
1	1	10	9	50.2
2	0.5	20	7	29.6
3	1.5	15	9	44.3
4	0.5	15	9	46.8
5	1	10	5	98.2
6	1.5	20	7	82.0
7	1.5	10	7	93.6
8	1	20	9	37.0
9	0.5	15	5	72.7
10	1	15	7	95.3
11	1.5	15	5	89.6
12	1	20	5	92.3
13	0.5	10	7	34.5

Table 2
RSM based significance level of the model and the model parameters

Significance value				
Response	Model	*A*	*B*	*C*
Total selenium removal	0.0094	0.0256	0.4677	0.0049

favor the accumulation of anionic selenium species onto 2LFh surface. The model factor *B* (initial selenocyanate concentration) shows *p*-value of 0.4677 that is greater than 0.05, suggesting no significant effect onto total selenium removal. Moreover, the analysis of variance (ANOVA) findings and model's significance level based on the probability (*p*) values was also probed. In general, the significance levels for the model and terms *A* and *C* were noted to be significant (i.e., less than 0.05). The effect of above-mentioned process parameters (i.e., *A*: 2LFh amount, *B*: initial selenocyanate concentration, and *C*: pH) on to overall selenium removal are shown in Figs. 11–13 and respective RSM model parameters are provided in Table 3. The model shows R^2 about 0.7040 indicating a modest fit model. Then, adjusted and the predicted R^2 values of 0.6054, and 0.4472, respectively, show the desired difference of less than 0.2. Furthermore, the average absolute deviation (AAD), which indicates the predictive capability of the developed model, is given by Eq. (8) [51].

$$\mathrm{AAD} = \left\{ \left[\sum_{i=1}^{p} \left(\frac{\left| y_{i,\mathrm{exp}} - y_{i,\mathrm{cal}} \right|}{y_{i,\mathrm{exp}}} \right) \right] / p \right\} \times 100 \tag{8}$$

where $y_{i,\mathrm{exp}}$ is the experimental responses, $y_{i,\mathrm{cal}}$ is the calculated responses, p is the number of experimental runs.

As the AAD value for the present model which is about 21.7% indicates a good fit [51]. Also, the adequate precision value (signal-to-noise ratio) is noted to be 8.1 and

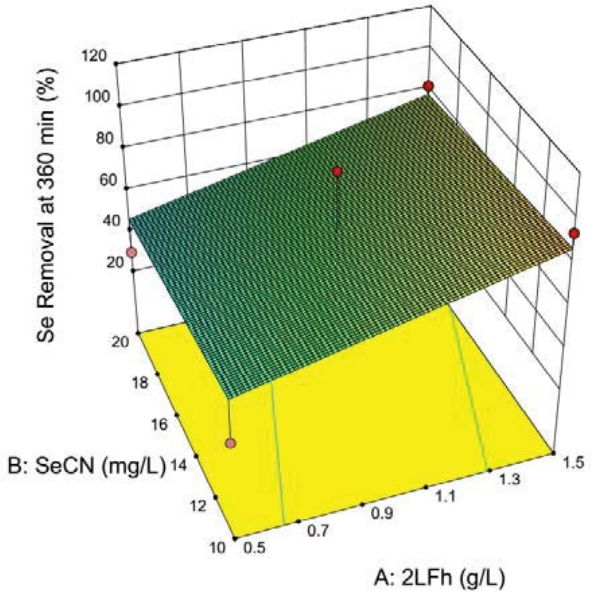

Fig. 11. 3D graph presenting the effect of 2LFh amount (A) and initial selenocyanate concentration and (B) on the removal of total selenium (1 g/L TiO_2 and pH 7).

is acceptable (as it is more than 4). These results show that the respective RSM based model can be employed for reasonable total selenium removal estimations. In summary, the combined TiO_2 photocatalysis and 2LFh adsorption system along with careful control of process parameters can be successfully applied to treat selenocyanate contaminated streams.

4. Conclusions

The TiO_2 photocatalysis cum 2LFh adsorption system was successfully applied for the removal of aqueous selenocyanate ($SeCN^-$) along with RSM based modeling for

Table 3
RSM based model characteristics

Response	Transformation	Adequate precision	R^2	Adjusted R^2	Predicted R^2	AAD (%)
Total selenium removal	None	8.123	0.7040	0.6054	0.4472	21.7

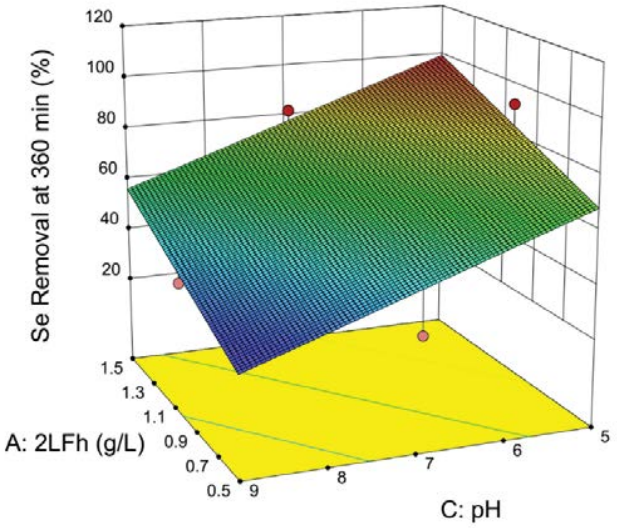

Fig. 12. 3D graph presenting the effect of 2LFh amount (A) and pH (C) on the removal of total selenium (20 mg/L selenocyanate and 1 g/L TiO_2).

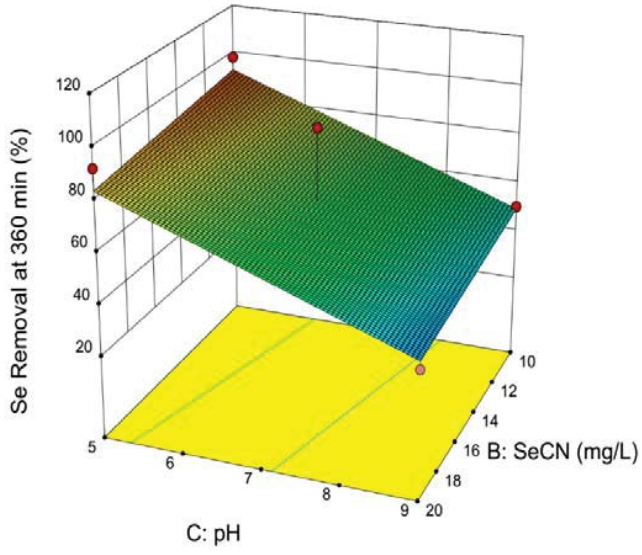

Fig. 13. 3D graph presenting the effect of initial selenocyanate concentration (B) and pH (C) on the removal of total selenium (1 g/L TiO_2 and 1 g/L 2LFh).

the total selenium removal under a varying set of process conditions. The TiO_2 based photocatalysis first oxidized the selenocyanate to selenite and selenate which were then removed via adsorption onto the 2LFh surface sites. The total selenium removal efficiency was noted to be higher at acidic pH values, whereas at basic pH values the selenium removal decreased. Considering the pH_{zpc} of 2LFh that is reported to be around ~8, the higher selenium removal at low pH values is attributed to respective cationic nature of 2LFh sites (Eq. (5)). However, as the 2LFh surface becomes more negatively charged with an increase in pH (Eq. (6)), it does not favor the adsorption of anionic selenium species because of an electrostatic repulsion. Furthermore, the noted reduced selenium removal at high pH values is also explained based on higher OH^- ion concentration and consequently its competitive adsorption on to respective 2LFh complexation sites. It is also anticipated that the differences in the types of surface complexes, that is, inner sphere vs. outer sphere, which the anionic selenate moiety forms with the 2LFh surface at low and high pH, respectively, also affects the degree of selenate removal.

Acknowledgments

The authors are thankful to the King Fahd University of Petroleum and Minerals (KFUPM) for providing all necessary support and infrastructure for this work. The authors are also thankful to the Deanship of Research (DSR-KFUPM) for the grant via SABIC Project # SB141004 and also to the Civil and Environmental Engineering Department (KFUPM) for providing the laboratory facilities.

References

[1] T.T.Y. Tan, D. Beydoun, R. Amal, Photocatalytic reduction of Se(VI) in aqueous solutions in UV/TiO_2 system: kinetic modeling and reaction mechanism, J. Phys. Chem. B., 107 (2003) 4296–4303.
[2] U. Tinggi, Essentiality and toxicity of selenium and its status in Australia: a review, Toxicol. Lett., 137 (2003) 103–110.
[3] S. Santos, G. Ungureanu, R. Boaventura, C. Botelho, Selenium contaminated waters: an overview of analytical methods, treatment options and recent advances in sorption methods, Sci. Total Environ., 521–522 (2015) 246–260.
[4] C.M. Stivanin de Almeida, A.S. Ribeiro, T.D. Saint'Pierre, N. Miekeley, Studies on the origin and transformation of selenium and its chemical species along the process of petroleum refining, Spectrochim. Acta, Part B, 64 (2009) 491–499.
[5] M.P. de Souza, I.J. Pickering, M. Walla, N. Terry, Selenium assimilation and volatilization from selenocyanate-treated Indian mustard and muskgrass, Plant Physiol., 128 (2002) 625–633.
[6] N. Miekeley, R.C. Pereira, E.A. Casartelli, A.C. Almeida, M. de F.B. Carvalho, Inorganic speciation analysis of selenium by ion chromatography-inductively coupled plasma-mass spectrometry and its application to effluents from a petroleum refinery, Spectrochim. Acta, Part B, 60 (2005) 633–641.
[7] G.B. Tonietto, J.M. Godoy, A.C. Oliveira, M.V. de Souza, Simultaneous speciation of arsenic (As(III), MMA, DMA, and As(V) and selenium (Se(IV), Se(VI), and $SeCN^-$) in petroleum refinery aqueous streams, Anal. Bioanal. Chem., 397 (2010) 1755–1761.
[8] D. Wallschlager, N.S. Bloom, Determination of selenite, selenate and selenocyanate in waters by ion chromatography-hydride

generation-atomic fluorescence spectrometry (IC-HG-AFS), J. Anal. At. Spectrom., 16 (2001) 1322–1328.
[9] N. Bleiman, Y.G. Mishael, Selenium removal from drinking water by adsorption to chitosan-clay composites and oxides: batch and columns tests, J. Hazard. Mater., 183 (2010) 590–595.
[10] Y.T. Chan, W.H. Kuan, T.Y. Chen, M.K. Wang, Adsorption mechanism of selenate and selenite on the binary oxide systems, Water Res., 43 (2009) 4412–4420.
[11] S. Das, M. Jim Hendry, J. Essilfie-Dughan, Adsorption of selenate onto ferrihydrite, goethite, and lepidocrocite under neutral pH conditions, Appl. Geochem., 28 (2013) 185–193.
[12] B.A. Labaran, M.S. Vohra, Competitive adsorption of selenite [Se(IV)], selenate [Se(VI)] and selenocyanate [$SeCN^-$] species onto TiO_2: experimental findings and surface complexation modelling, Desal. Water Treat., 124 (2018) 267–278.
[13] K.H. Goh, T.T. Lim, Geochemistry of inorganic arsenic and selenium in a tropical soil: effect of reaction time, pH, and competitive anions on arsenic and selenium adsorption, Chemosphere, 55 (2004) 849–859.
[14] B.A. Labaran, M.S. Vohra, Photocatalytic removal of selenite and selenate species: effect of EDTA and other process variables, Environ. Technol., 35 (2014) 1091–1100.
[15] M.S. Vohra, M.S. Al-Suwaiyan, M.H. Essa, M.M.I. Chowdhury, M.M. Rahman, B.A. Labaran, Application of solar photocatalysis and solar photo-Fenton processes for the removal of some critical charged pollutants: mineralization trends and formation of reaction intermediates, Arabian J. Sci. Eng., 41 (2016) 3877–3887.
[16] B.A. Labaran, M.S. Vohra, Solar photocatalytic removal of selenite, selenate, and selenocyanate species, Clean Soil Air Water, 45 (2017), doi: 10.1002/clen.201600268.
[17] M.S. Vohra, B.A. Labaran, Photocatalytic treatment of mixed selenocyanate and phenol streams: process modeling, optimization, and kinetics, Environ. Prog. Sustainable Energy, 39 (2020) 1–11.
[18] M.S. Vohra, Selenocyanate ($SeCN^-$) contaminated wastewater treatment using TiO_2 photocatalysis: $SeCN^-$ complex destruction, intermediates formation, and removal of selenium species, Fresenius Environ. Bull., 24 (2015) 1108–1118.
[19] T.S. Kazeem, B.A. Labaran, H. Ahmed, T. Mohammed, M.H. Essa, M.S. Al-Suwaiyan, M.S. Vohra, Treatment of aqueous selenocyanate anions using electrocoagulation, Int. J. Electrochem. Sci., 14 (2019) 10538–10564.
[20] J. Das, D. Das, G.P. Dash, K.M. Parida, Studies on Mg/Fe hydrotalcite-like-compound (HTlc): I. Removal of inorganic selenite (SeO_3^{2-}) from aqueous medium, J. Colloid Interface Sci., 251 (2002) 26–32.
[21] X. Meng, S. Bang, G.P. Korfiatis, Removal of selenocyanate from water using elemental iron, Water Res., 36 (2002) 3867–3873.
[22] S.D. Overman, Process for Removing Selenium from Refinery Process Water and Waste Water Streams, U.S. Patent 5,993,667 (WO-1999020569-A1), 1999.
[23] D. Peak, D.L. Sparks, Mechanisms of selenate adsorption on iron oxides and hydroxides, Environ. Sci. Technol., 36 (2002) 1460–1466.
[24] M.MV. Snyder, W. Um, Adsorption mechanisms and transport behavior between selenate and selenite on different sorbents, Int. J. Waste Resour., 4 (2014), doi: 10.4172/2252–5211.1000144.
[25] K. Atmatzidis, F. Alimohammadi, D.R. Strongin, R. Tehrani, Biomimetic system for the application of nanomaterials in fluid purification: removal of arsenic with ferrihydrite, ACS Omega, 5 (2020) 5873–5880.
[26] A.C. Dias, M.P.F. Fontes, C. Reis, C.R. Bellato, S. Fendorf, Simplex-centroid mixture design applied to arsenic(V) removal from waters using synthetic minerals, J. Environ. Manage., 238 (2019) 92–101.
[27] S. Kim, W.C. Lee, H.G. Cho, B. Lee, P. Lee, S.H. Choi, Equilibria, kinetics, and spectroscopic analyses on the uptake of aqueous arsenite by two-line ferrihydrite, Environ. Technol., 35 (2014) 251–261.
[28] A.A. Kumar, A. Som, P. Longo, C. Sudhakar, R.G. Bhuin, S.S. Gupta, Anshup, M.U. Sankar, A. Chaudhary, R. Kumar, T. Pradeep, Confined metastable 2-Line ferrihydrite for affordable point-of-use arsenic-free drinking water, Adv. Mater., 29 (2017), doi: 10.1002/adma.201604260.
[29] W.C. Lee, S. Kim, J. Ranville, S. Yun, S.H. Choi, Sequestration of arsenate from aqueous solution using 2-line ferrihydrite : equilibria, kinetics, and X-ray absorption spectroscopic analysis, Environ. Earth Sci., 71 (2014) 3307–3318.
[30] X. Jiang, C. Peng, D. Fu, Z. Chen, L. Shen, Q. Li, T. Ouyang, Y. Wang, Removal of arsenate by ferrihydrite via surface complexation and surface precipitation, Appl. Surf. Sci., 353 (2015) 1087–1094.
[31] W. Xiu, H. Guo, X. Zhou, R.B. Wanty, M. Kersten, Applied geochemistry change of arsenite adsorption mechanism during aging of 2-line ferrihydrite in the absence of oxygen, Appl. Geochem., 88 (2018) 149–157.
[32] F. Frau, D. Addari, D. Atzei, R. Biddau, R. Cidu, A. Rossi, Influence of major anions on As(V) adsorption by synthetic 2-line ferrihydrite. Kinetic investigation and XPS study of the competitive effect of bicarbonate, Water Air Soil Pollut., 205 (2010) 25–41.
[33] C. Wang, Y. Cui, J. Zhang, M. Gomez, S. Wang, Y. Jia, Chemosphere occurrence state of co-existing arsenate and nickel ions at the ferrihydrite-water interface: mechanisms of surface complexation and surface precipitation via ATR-IR spectroscopy, Chemosphere, 206 (2018) 33–42.
[34] A. Dzieniszewska, J. Kyziol-komosinska, M. Pająk, Adsorption and bonding strength of chromium species by ferrihydrite from acidic aqueous solutions, Peer J., 9324 (2020), doi: 10.7717/peerj.9324.
[35] L. Zhu, F. Fu, B. Tang, Three-dimensional transfer of Cr(VI) co-precipitated with ferrihydrite containing silicate and its redistribution and retention during aging, Sci. Total Environ., 696 (2019), doi: 10.1016/j.scitotenv.2019.133966.
[36] M. Villacís-García, M. Ugalde-Arzate, K. Vaca-Escobar, M. Villalobos, R. Zanella, N. Martínez-Villegas, Laboratory synthesis of goethite and ferrihydrite of controlled particle sizes, Bol. Soc. Geol. Mex., 67 (2015) 433–446.
[37] N. Finck, M. Bouby, K. Dardenne, Fate of Lu(III) sorbed on 2-line ferrihydrite at pH 5.7 and aged for 12 years at room temperature. I: insights from ICP-OES, XRD, ESEM, AsFlFFF/ICP-MS, and EXAFS spectroscopy, Environ. Sci. Pollut. Res., 26 (2019) 5238–5250.
[38] T. Yokosawa, E. Prestat, R. Polly, M. Bouby, K. Dardenne, N. Finck, S.J. Haigh, M.A. Denecke, H. Geckeis, Fate of Lu(III) sorbed on 2-line ferrihydrite at pH 5. 7 and aged for 12 years at room temperature. II: insights from STEM-EDXS and DFT calculations, Environ. Sci. Pollut. Res., 26 (2019) 5282–5293.
[39] N. Abdus-Salam, F.A. M'civer, Synthesis, characterisation and application of 2-line and 6-line ferrihydrite to Pb(II) removal from aqueous solution, J. Appl. Sci. Environ. Manage., 16 (2012) 327–336.
[40] K. Rout, M. Mohapatra, S. Anand, 2-Line ferrihydrite: synthesis, characterization and its adsorption behaviour for removal of Pb(II), Cd(II), Cu(II) and Zn(II) from aqueous solutions, Dalton Trans., 41 (2012) 3302–3312.
[41] B. Zhu, Y. Jia, Z. Jin, B. Sun, T. Luo, L. Kong, J. Liu, A facile precipitation synthesis of mesoporous 2-line ferrihydrite with good fluoride removal, RSC Adv., 5 (2015) 84389–84397.
[42] L. Brinza, H.P. Vu, M. Neamtu, L.G. Benning, Experimental and simulation results of the adsorption of Mo and V onto ferrihydrite, Sci. Rep., 9 (2019) 1–12.
[43] L. Zhao, J. Basly, M. Baudu, Macroporous alginate/ferrihydrite hybrid beads used to remove anionic dye in batch and fixed-bed reactors, J. Taiwan Inst. Chem. Eng., 74 (2017) 129–135.
[44] T. Mathew, K. Suzuki, Y. Nagai, T. Nonaka, Y. Ikuta, N. Takahashi, N. Suzuki, H. Shinjoh, Mesoporous 2-line ferrihydrite by a solution-phase cooperative assembly process for removal of organic contaminants in air, Chem. Eur. J., 17 (2011) 1092–1095.
[45] D.B. Hausner, N. Bhandari, A.M. Pierre-Louis, J.D. Kubicki, D.R. Strongin, Ferrihydrite reactivity toward carbon dioxide, J. Colloid Interface Sci., 337 (2009) 492–500.
[46] T. Mathew, K. Suzuki, Y. Ikuta, Y. Nagai, N. Takahashi, H. Shinjoh, Mesoporous ferrihydrite-based iron oxide nano-

particles as highly promising materials for ozone removal, Angew. Chem. Int. Ed., 123 (2011) 7519–7522.
[47] F.E. Rhoton, J.M. Bigham, Phosphate adsorption by ferrihydrite-amended soils, J. Environ. Qual., 34 (2005) 890–896.
[48] H.P. Vu, J.W. Moreau, Thiocyanate adsorption on ferrihydrite and its fate during ferrihydrite transformation to hematite and goethite, Chemosphere, 119 (2015) 987–993.
[49] K. Mitchell, R.M. Couture, T.M. Johnson, P.R.D. Mason, P. Van Cappellen, Selenium sorption and isotope fractionation: iron(III) oxides versus iron(II) sulfides, Chem. Geol., 342 (2013) 21–28.
[50] S. Wang, L. Lei, D. Zhang, G. Zhang, R. Cao, X. Wang, J. Lin, Y. Jia, Stabilization and transformation of selenium during the Fe(II)-induced transformation of Se(IV)-adsorbed ferrihydrite under anaerobic conditions, J. Hazard. Mater., 384 (2020), doi: 10.1016/j.jhazmat.2019.121365.
[51] D. Baş, İ.H. Boyacı, Modeling and optimization I: usability of response surface methodology, J. Food Eng., 78 (2007) 836–845.
[52] T. Mohammed, T.S. Kazeem, M.H. Essa, B.A. Labaran, M.S. Vohra, Comparative study on electrochemical treatment of arsenite: effects of process parameters, sludge characterization and kinetics, Arabian J. Sci. Eng., 45 (2020) 3799–3815.
[53] B.A. Labaran, M.S. Vohra, Application of activated carbon produced from phosphoric acid-based chemical activation of oil fly ash for the removal of some charged aqueous phase dyes: role of surface charge, adsorption kinetics, and modeling, Desal. Water Treat., 57 (2016) 16034–16052.
[54] C. Rani, S.D. Tiwari, Phase transitions in two-line ferrihydrite nanoparticles, Appl. Phys. A, 123 (2017) 1–4.
[55] C.L. Snow, K.I. Lilova, A.V. Radha, Q. Shi, S. Smith, A. Navrotsky, J. Boerio-Goates, B.F. Woodfield, Heat capacity and thermodynamics of a synthetic two-line ferrihydrite, J. Chem. Thermodyn., 58 (2013) 307–314.
[56] R. Brayner, T. Coradin, P. Beaunier, J. Grenèche, C. Djediat, C. Yéprémian, A. Couté, F. Fiévet, Intracellular biosynthesis of superparamagnetic 2-lines ferri-hydrite nanoparticles using *Euglena gracilis* microalgae, Colloids Surf., B, 93 (2012) 20–23.
[57] S. Jeong, K. Yang, E.H. Jho, K. Nam, Importance of chemical binding type between As and iron-oxide on bioaccessibility in soil: test with synthesized two line ferrihydrite, J. Hazard. Mater., 330 (2017) 157–164.
[58] Y. Jia, B. Zhu, K. Zhang, Z. Jin, B. Sun, T. Luo, X. Yu, L. Kong, J. Liu, Porous 2-line ferrihydrite/bayerite composites (LFBC): fluoride removal performance and mechanism, Chem. Eng. J., 268 (2015) 325–336.
[59] Y. Huang, S. Zhang, C. Liu, H. Lu, S. Ni, X. Cheng, Z. Long, R. Wang, Transformations of 2-line ferrihydrite and its effect on cadmium adsorption, Environ. Sci. Pollut. Res., 25 (2018) 18059–18070.
[60] M.R. Hoffmann, S.T. Martin, W.C. Choi, D.W, Bahnemann, Environmental applications of semiconductor photocatalysis, Chem. Rev., 95 (1995) 69–96.
[61] F. Juillot, C. Marechal, M. Ponthieu, S. Cacaly, G. Morin, M. Benedetti, J.L. Hazemann, O. Proux, F. Guyot, Zn isotopic fractionation caused by sorption on goethite and 2-Lines ferrihydrite, Geochim. Cosmochim. Acta, 72 (2008) 4886–4900.
[62] A.A. Mamun, M. Morita, M. Matsuoka, C. Tokoro, Sorption mechanisms of chromate with coprecipitated ferrihydrite in aqueous solution, J. Hazard. Mater., 334 (2017) 142–149.